ELSEVIER

Physics Letters B 541 (2002) 234–242

PHYSICS LETTERS B

www.elsevier.com/locate/npe

Measurements of atmospheric muon spectra at mountain altitude

T. Sanuki [a,*], M. Fujikawa [a], K. Abe [a], K. Anraku [a,1], Y. Asaoka [a,2], H. Fuke [a], S. Haino [a], M. Imori [a], K. Izumi [a], T. Maeno [b], Y. Makida [c], N. Matsui [a], H. Matsumoto [a], H. Matsunaga [a,3], M. Motoki [a,4], J. Nishimura [a], M. Nozaki [b], S. Orito [a,5], M. Sasaki [c,6], Y. Shikaze [b], T. Sonoda [a], J. Suzuki [c], K. Tanaka [c], Y. Toki [b], A. Yamamoto [c], Y. Yamamoto [a], K. Yamato [b], T. Yoshida [c], K. Yoshimura [c]

[a] *The University of Tokyo, Bunkyo, Tokyo 113-0033, Japan*
[b] *Kobe University, Kobe, Hyogo 657-8501, Japan*
[c] *High Energy Accelerator Research Organization (KEK), Tsukuba, Ibaraki 305-0801, Japan*

Received 24 May 2002; received in revised form 3 July 2002; accepted 5 July 2002

Editor: L. Rolandi

Abstract

We report new measurements of absolute fluxes of atmospheric muons at mountain altitude. The measurements were carried out with the BESS detector at the top of Mt. Norikura, 2 770 m above sea level, in Japan. The overall errors were less than 10%. The measured results are discussed in comparison with theoretical calculations. © 2002 Elsevier Science B.V. All rights reserved.

PACS: 95.85.Ry; 96.40.Tv

Keywords: Atmospheric muon; Atmospheric neutrino; Superconducting spectrometer

1. Introduction

Atmospheric muons observed in the deep atmosphere are carrying information on the interaction of primary and secondary cosmic-ray particles in the atmosphere. Since decay probability and energy loss rate depend on energy, high-statistics measurement of spectral shape can provide useful knowledge to understand propagation process of cosmic-ray particles through the atmosphere. For a more detailed study of neutrino oscillation phenomena observed in atmospheric neutrinos it is essentially important to reduce the systematic errors in the predicted energy spectra of neutrinos. In order to improve the accu-

* Corresponding author.
E-mail address: sanuki@phys.s.u-tokyo.ac.jp (T. Sanuki).

[1] Present address: Kanagawa University, Yokohama, Kanagawa 221-8686, Japan.

[2] Present address: ICRR, The University of Tokyo, Kashiwa, Chiba 227-8582, Japan.

[3] Present address: University of Tsukuba, Tsukuba, Ibaraki 305-8571, Japan.

[4] Present address: Tohoku University, Sendai, Miyagi 980-8578, Japan.

[5] Deceased.

[6] Present address: National Aeronautics and Space Administration, Goddard Space Flight Center, Greenbelt, MD 20771, USA; NAS/NRC Research Associate.

0370-2693/02/$ – see front matter
PII: S0370-2693(02)02265-7

racy of the predictions, a detailed understanding of hadronic interactions, as well as precise information of primary cosmic-ray fluxes, is indispensable. As for absolute fluxes of cosmic-ray protons and helium nuclei below 100 GeV, a very precise measurement was carried out by using the BESS detector [1]. Two independent experiments, the AMS [2,3] and the BESS, show extremely good agreement with each others in their results. Since production and decay process of muons are accompanied by neutrino productions, the muons fluxes correlate directly to the hadronic interactions. Thus the precise measurement of atmospheric muon spectra can also provide important information to improve accuracy of atmospheric neutrino calculations.

We measured absolute fluxes of atmospheric muons at the top of Mt. Norikura, Japan with the BESS detector, which was the same apparatus as we utilized to measure sea-level muons [4] as well as the primary protons and helium nuclei [1]. These measurements provide fundamental and very useful information about hadronic interactions and geomagnetic effects.

2. BESS experiment

2.1. BESS detector

The BESS (Balloon-borne Experiment with a Superconducting Spectrometer) detector [5–9] is a high-resolution spectrometer with a large acceptance to perform highly sensitive searches for rare cosmic-ray components, and precise measurement of the absolute fluxes of various cosmic rays. Fig. 1 shows a schematic cross-sectional view of the BESS instrument. In the central region, a uniform magnetic field of 1 Tesla is provided by using a thin superconducting solenoidal coil. A magnetic-rigidity ($R \equiv Pc/Ze$) of an incoming charged particle is measured by a tracking system, which consists of a jet-type drift chamber (JET) and two inner-drift-chambers (IDCs) inside the magnetic field. The deflection (R^{-1}) and its error are calculated for each event by applying a circular fitting using up-to 28 hit points, each with a spatial resolution of 200 μm. The maximum detectable rigidity (MDR) was estimated to be 200 GV. Time-of-flight (TOF) hodoscopes provide the velocity (β) and energy loss ($\mathrm{d}E/\mathrm{d}x$) measurements. A $1/\beta$ resolution of 1.6% was achieved in this experiment.

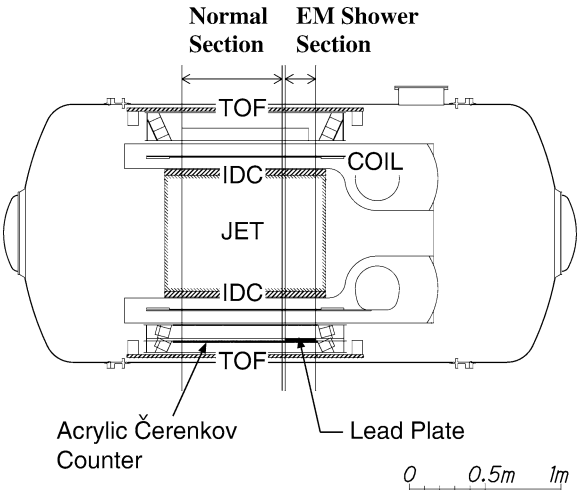

Fig. 1. Schematic cross-sectional view of the BESS instrument.

Particle identification was made by requiring proper $1/\beta$ as well as $\mathrm{d}E/\mathrm{d}x$ as a function of the rigidity. An electromagnetic shower counter has been equipped for electron/muon separation. It consists of a 2 X_0 thick lead plate and an acrylic Čerenkov counter. The lead plate covers about 1/5 of the total acceptance.

The simple cylindrical shape and the uniform magnetic field make it simple and reliable to determine the geometrical acceptance precisely. The live data-taking time was measured exactly by counting 1 MHz clock pulses with a scaler system gated by a "ready" status that controls the first-level trigger. The resultant live-time ratio was as high as 98.8% through the measurement.

2.2. Data samples

The atmospheric cosmic-ray events were observed at Norikura Observatory, ICRR, the University of Tokyo, Japan. It is located at $36°06'N, 137°33'E$, which is about 40 km southeast of Kamioka. The altitude is 2 770 m above sea level. The vertical geomagnetic cutoff rigidity is 11.2 GV [10]. The experiment was performed during two periods of 17th–19th and 21st–23th of September 1999. During the observation, the atmospheric pressure and temperature varied as shown in Fig. 2. The mean (root-mean-square) atmospheric pressure and temperature were

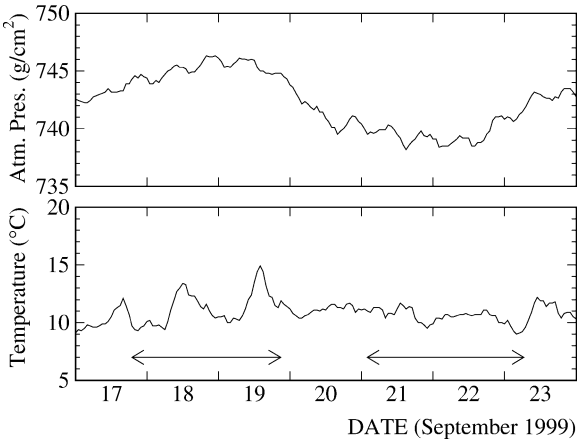

Fig. 2. Atmospheric pressure and temperature during the observation. The experiment was performed during two periods of 17th–19th and 21st–23th.

742.4(2.9) g/cm^2 and 10.9(1.1) °C, respectively. The total live data-taking time was about 4 days.

3. Data analysis

3.1. Data reduction

In this analysis, the BESS detector was divided into two sections as shown in Fig. 1; i.e., the "normal" section and the "EM shower" section. The EM shower section includes the shower counter. The normal section was used to measure muon momentum spectra. In order to estimate small contaminations of electrons, the data samples recorded in the EM shower section were examined.

In the first stage of data reduction, we selected events with a single-track fully contained within a fiducial volume. The fiducial volume was defined as a central region in the JET chamber. This definition ensured the longest track to achieve the highest resolution in the rigidity measurement. The zenith angle (θ_z) was limited to be $\cos\theta_z \geqslant 0.98$ to obtain near vertical fluxes. The single-track event was defined as an event which has only one isolated track and one or two hit-counters in each layer of the TOF hodoscopes. Since the major component of the observed particles was muons, those which can easily penetrate the detector, almost all particles passed this selection criterion. The single-track selection eliminated very rare interacting

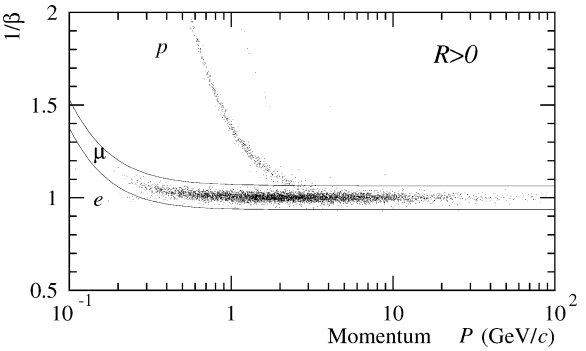

Fig. 3. Positive muon selection in $1/\beta$ vs. momentum. Muons were selected with a high efficiency. Proton and positron contaminations were subtracted.

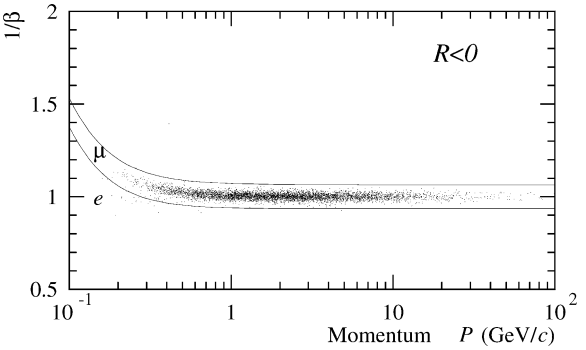

Fig. 4. Negative muon selection in $1/\beta$ vs. momentum. Muons were selected with a high efficiency. Electron contamination was subtracted.

events. In order to verify the selection, events were scanned randomly. It was confirmed that 1 995 out of 2 000 visually-identified single-track events passed this selection criteria and interacting events were fully eliminated. Thus, the track reconstruction efficiency was determined to be $99.8 \pm 0.1\%$ for the single-track event. The single-track events selected in this stage were followed by the succeeding analysis.

The $\mathrm{d}E/\mathrm{d}x$ inside the TOF hodoscope was examined to ensure that the particle was singly charged. The particle identification was performed by requiring proper $1/\beta$ as a function of the momentum as shown in Figs. 3 and 4. Since the $1/\beta$ distribution was well described by Gaussian and a half width of the $1/\beta$ selection band was set at 3.89σ, the efficiency was very close to unity. Taking into account

a small deviation from pure Gaussian, the efficiency was evaluated to be 99.9%. In order to assure accuracy of the momentum measurement, event qualities such as χ^2 in the track fitting procedure were required. The efficiency of this quality-check was evaluated to be $96.3 \pm 0.1\%$ as a ratio of the number of good quality events to all events between 10 and 20 GeV/c. Since the quality-check required consistency between the fitted track and each hit in the tracking detector, its efficiency does not depend on the momentum in higher momentum region where multiple scattering can be neglected. Accordingly the above value of the quality-check efficiency was applied to higher momentum region. Before and after the quality-check and succeeding correction of its efficiency, the obtained flux above 10 GeV/c changed no more than $\pm 2.2\%$. These changes were treated as systematic errors in the quality-check. Below 10 GeV/c, quality-check was not imposed, because momentum resolution before the quality-check was high enough to measure the momentum. Thus there was no systematic error associated with the quality-check.

With the data reduction described above, 707 563 muon candidates were selected. The combined efficiency in the data reduction process was $99.6 \pm 0.1\%$ and $95.8 \pm 2.2\%$ below and above 10 GeV/c, respectively.

3.2. Contamination estimation

As seen in Figs. 3 and 4, main background sources were protons for positively charged muons whereas electrons and positrons for both positively and negatively charged muons. Protons were identified by examining $1/\beta$ distribution. Below 1.6 GeV/c, protons were clearly separated from muons. Between 1.6 and 3.2 GeV/c, the proton contamination in the muon candidates and its error were estimated by fitting the $1/\beta$ distribution with a double-Gaussian function as shown in Fig. 5. The ratio of observed protons to muons was found to be well described as a simple power law as $p/\mu^+ = 0.24\, P^{-0.80}$ in a momentum region of 1–3 GeV/c. The proton contamination above 3 GeV/c was estimated by extrapolating this power law. Above around 10 GeV/c, however, the p/μ^+ ratio will be constant. It is reasonably assumed that pions are produced having a similar spectral index of the parent protons and then decay to muons, those which can reach the mountain altitude before they decay in a higher momentum region. Under this assumption, the spectral index of muons is similar to that of the parent protons, resulting in a constant p/μ^+ ratio. This tendency was well reproduced by two Monte Carlo simulations [11]; one simulation incorporated the FRITIOF7 [12] as a hadronic interaction model and the other was developed based on the DPMJET-III event generator [13]. In this analysis, the p/μ^+ ratio above 10 GeV/c was assumed to take a constant value of 3.8%. These proton contaminations were subtracted from the muon candidates. An error originated from the proton subtraction between 1.6 and 3.2 GeV/c was estimated during the fitting procedure to be less than 1%. In a higher momentum region, the p/μ^+ ratios predicted by the two Monte Carlo simulations agreed with each other within $\pm 1\%$. These discrepancies were included into systematic errors.

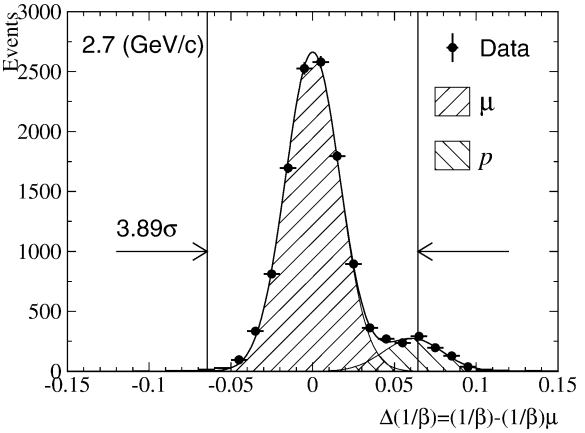

Fig. 5. An estimation of proton contamination by TOF information. Muons have a peak at $\Delta(1/\beta) = 0$. Filled circles are data at around 2.7 GeV/c. Best fitting curves are also shown.

The muon candidates might include pion contamination, since it has the same signature and is hardly identified. According to the same Monte Carlo simulations that was utilized for p/μ^+ ratio estimations, π/μ ratio was estimated to be less than 1% below 40 GeV/c and less than 3% between 40 and 100 GeV/c. It is smaller than the statistical errors over the whole momentum range in this analysis. The pions

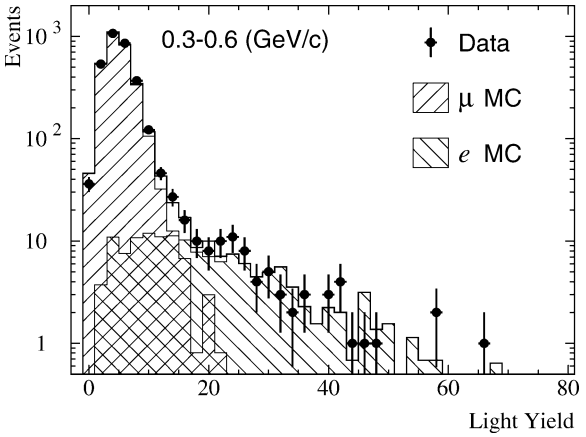

Fig. 6. An estimation of electron contamination in events of the shower counter. Filled circles are data between 0.3 and 0.6 GeV/c. Histograms show the best fit Monte Carlo data.

were neglected in this analysis both in contamination subtraction and systematic error estimation.

The electron contamination was to be considered as a background well below 1 GeV/c. For an estimation of electron contamination, events passed through the EM shower section were considered. The Čerenkov light yield from the shower counter was examined to estimate an e/μ ratio. Fig. 6 demonstrates the following estimation procedure. The Čerenkov light yields for electrons and muons were individually obtained from Monte Carlo simulations. The observed light output distribution is a sum of these two distributions with appropriate weights. By changing weights for those two distributions, the best fit e/μ ratio was obtained. The electron contamination in the muon candidates observed in the EM shower section was about 1.5% at 0.6 GeV/c and rapidly decreased with increasing momentum. The e/μ ratio below 1 GeV/c was found to be described as $e/\mu = 0.0024\,P^{-3.7}$. Above 1 GeV/c, the number of observed electron events was too small to estimate its ratio by this procedure. We estimated the electron contamination by extrapolating the ratio obtained below 1 GeV/c to a higher momentum region. After correcting the different data reduction efficiency in the normal section from that in the EM shower section by using the Monte Carlo simulations, the electron contamination was subtracted from the muon candidates observed in the normal section. Accuracy of the electron subtraction was limited by poor statistics of electron events. An error in this subtraction was estimated from the fitting procedure to be 1.0% at 0.6 GeV/c and rapidly decrease with increasing momentum.

The proton contamination was to be properly subtracted above a few GeV/c. On the other hand, the electron contamination should be carefully considered and properly subtracted in a different momentum region below 1 GeV/c. Thus the overall error in the contamination subtraction was as small as 1% over the whole momentum range. It may be worth mentioning that e/μ and p/μ ratios discussed above are different from flux ratios because the efficiencies for protons and electrons are not same as that for muons.

3.3. Corrections

In order to determine the atmospheric muon spectra at the mountain altitude, the following corrections are required; (i) exposure factor, (ii) ionization energy loss, and (iii) interaction loss.

The exposure factor is a product of geometrical acceptance and live-time. The geometrical acceptance defined for this analysis was calculated by simulation technique [14] to be 0.0214 $\mathrm{m}^2\,\mathrm{sr}$ for energetic particles which have straight track inside the tracking volume. It was almost constant over the whole momentum range. The simple cylindrical shape and the uniform magnetic field make it simple and reliable to determine the geometrical acceptance precisely. The error arose from uncertainty of the detector alignment was estimated to be 0.4%. Between observed and simulated zenith angular distributions of the trajectories, a small discrepancy was found below 2 GeV/c. In the simulation isotropic trajectories were generated to obtain the geometrical acceptance, however, the flux of atmospheric muons has a zenith angle dependence. In a low momentum region, the dependence might be significant even in the so near vertical direction as $\cos\theta_z \geqslant 0.98$. The discrepancy was included in the systematic errors. The systematic error associated with this discrepancy was estimated to be 3.5% at 0.6 GeV/c and decreased with increasing momentum. The live data-taking time was measured exactly to be 339 874 seconds.

The energy of each particle at the top of the instrument was calculated by summing up the ionization en-

ergy losses inside the instrument with tracing back the event trajectory.

In order to estimate the interaction loss probabilities inside the BESS detector, Monte Carlo simulations with the GEANT code [15] were performed. The probabilities that muons can be identified as single-track events were evaluated by applying the same selection criterion to the Monte Carlo events. The resultant single-track efficiency was 97.9% at 10 GeV/c and almost constant over the momentum region discussed here. The Monte Carlo simulation of the BESS detector well reproduced the observed event profile. By comparing the observed and simulated parameters used in the single-track selection, i.e., the number of tracks inside the tracking volume and the number of hit-counters in each layer of the TOF hodoscopes, it was concluded that a discrepancy between the observed and simulated event shapes was no more than $\pm 1.6\%$ in the whole momentum range discussed here. This discrepancy was included in the systematic error of the single-track efficiency. Another source of the systematic error in the Monte Carlo simulation was uncertainty of the material distribution inside the BESS detector, which was estimated to be $\pm 10\%$. Since the single-track efficiency was as high as 98%, the systematic error originated from this uncertainty was as small as 0.2%.

The combined systematic errors obtained by quadratically adding the uncertainties were ± 3.0, ± 1.4, and $\pm 1.7\%$ at 1, 10, and 100 GeV/c, respectively.

3.4. Spectrum deformation effect

Because of the finite resolution in the rigidity measurement and the steep spectral shape, the observed spectrum may suffer deformation. In a low rigidity region well below the MDR, the spectrum deformation is negligibly small. In a higher rigidity region, however, a deflection becomes comparable to an error in curvature measurement; thus, the spectrum deformation is to be considered. This spectrum deformation effect of the BESS detector was discussed in our previous paper [1]. According to the discussion, the effect was estimated to be no more than 3% below 120 GeV/c. The deformation effect is smaller than the statistical errors over the whole momentum range in this analysis. Thus no correction was applied to the measured spectra.

4. Results and discussions

The momentum spectra of the atmospheric muons in momentum ranges of 0.6 through 106 GeV/c at a mountain altitude of 2 770 m above sea level have been measured with the BESS detector. The results are summarized in Table 1 and shown in Fig. 7. The first and second errors in Table 1 represent statistical and systematic errors, respectively. The overall errors including both errors are less than $\pm 10\%$. In Fig. 7, our result is compared with other absolute flux measurements [4,16,17]. A discrepancy between the observed muon fluxes is mainly due to the difference in altitudes.

Fig. 8 shows charge ratios of atmospheric muons observed in a series of muon measurements with the BESS detector. The big difference in the charge ratios observed in Japan and Canada comes from the influence of the geomagnetic cutoff rigidity as discussed in Ref. [4]. Below 10 GeV/c, the charge ratio at mountain altitude is slightly lower than that at sea level. This tendency was made by energy loss inside the atmosphere between mountain altitude and sea-level. In a higher momentum region, the ratio seems to approach to around 1.28.

Our results were compared with theoretical predictions, in which atmospheric muon spectra were calculated simultaneously with atmospheric neutrinos. Fig. 9 shows comparisons between our results and the predictions. The predicted spectra were calculated based on Ref. [18], but some parameters, such as atmospheric pressure, temperature and zenith angle limit, were adjusted to reproduce the experimental conditions. In Ref. [18], two calculations were discussed; one was developed on the basis of the HKKM interaction model [19] and the other was calculated by employing the DPMJET-III event generator [13] as hadronic interaction models. As Fig. 9 indicates, the DPMJET-III interaction model reproduced the observed spectra better than the HKKM interaction model. Some deviation, however, was found between the observed and calculated spectra especially below 1 GeV/c. It seems reasonable to suppose that the hadronic interaction models are to be tested and improved by accurate spectra of atmospheric muons. The precise measurement of atmospheric secondary particles will improve the accuracy in the atmospheric neutrino calculations.

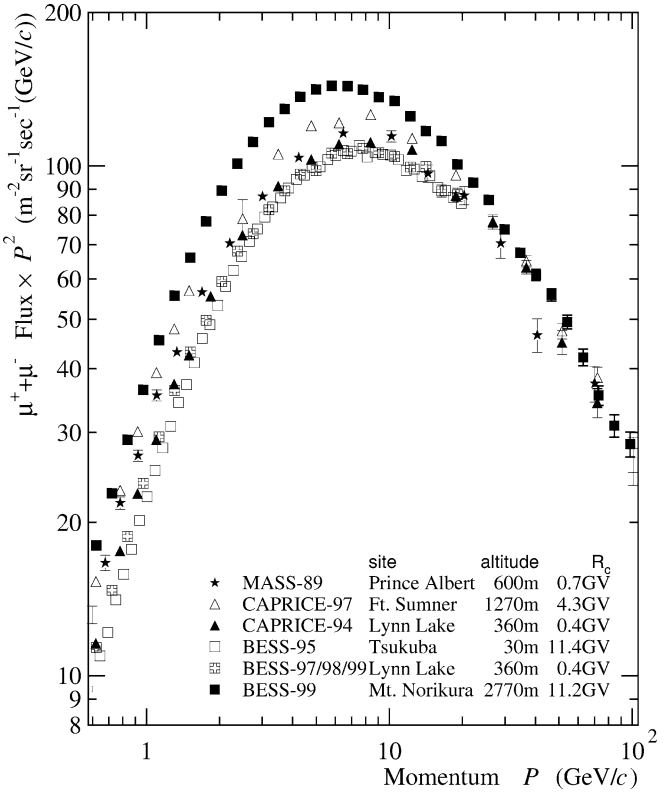

Fig. 7. Absolute differential momentum spectra of atmospheric muons. Vertical axis shows the sum of μ^+ and μ^- fluxes multiplied by P^2. Only statistical errors are included. The geomagnetic cutoff rigidity at each site is shown as R_c. The difference among the fluxes is mainly due to the difference in altitudes.

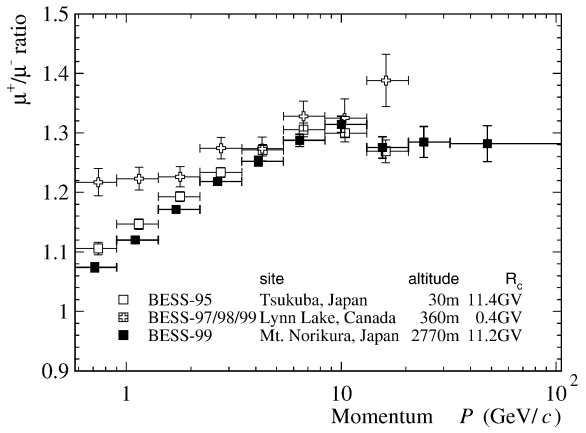

Fig. 8. Charge ratios of atmospheric muons. Only statistical errors are included. The geomagnetic cutoff rigidity at each site is shown as R_c. The difference among the ratios is caused by the difference in geomagnetic cutoff rigidity and energy loss inside the atmosphere.

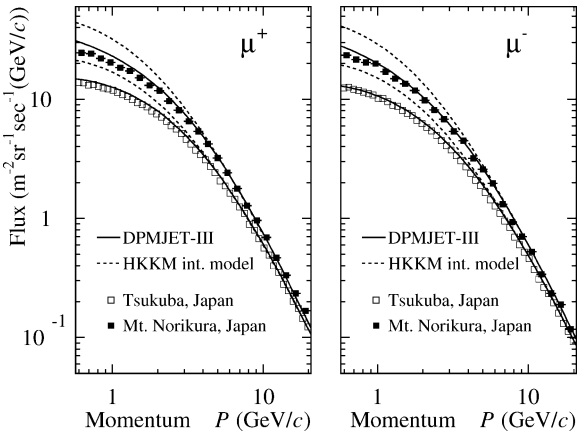

Fig. 9. Comparison between the observed and calculated spectra of atmospheric muons. The calculation with the DPMJET-III event generator reproduced our results better than the HKKM interaction model.

Table 1
Absolute differential momentum spectra of atmospheric muons

Momentum range GeV/c	μ^+		μ^-	
	$\overline{P}$ GeV/c	Flux $\pm \Delta\text{Flux}_{\text{sta}} \pm \Delta\text{Flux}_{\text{sys}}$ $(\text{m}^2\,\text{sr}\,\text{s}\,\text{GeV}/c)^{-1}$	$\overline{P}$ GeV/c	Flux $\pm \Delta\text{Flux}_{\text{sta}} \pm \Delta\text{Flux}_{\text{sys}}$ $(\text{m}^2\,\text{sr}\,\text{s}\,\text{GeV}/c)^{-1}$
0.576–0.669	0.595	$2.39 \pm 0.02 \pm 0.09 \times 10$	0.603	$2.29 \pm 0.02 \pm 0.09 \times 10$
0.669–0.776	0.693	$2.29 \pm 0.02 \pm 0.08 \times 10$	0.697	$2.11 \pm 0.02 \pm 0.07 \times 10$
0.776–0.901	0.806	$2.17 \pm 0.02 \pm 0.07 \times 10$	0.807	$1.99 \pm 0.02 \pm 0.06 \times 10$
0.901–1.05	0.930	$2.03 \pm 0.02 \pm 0.06 \times 10$	0.938	$1.83 \pm 0.01 \pm 0.05 \times 10$
1.05–1.21	1.08	$1.89 \pm 0.01 \pm 0.05 \times 10$	1.08	$1.70 \pm 0.01 \pm 0.05 \times 10$
1.21–1.41	1.25	$1.73 \pm 0.01 \pm 0.05 \times 10$	1.26	$1.53 \pm 0.01 \pm 0.04 \times 10$
1.41–1.63	1.45	$1.54 \pm 0.01 \pm 0.04 \times 10$	1.46	$1.33 \pm 0.01 \pm 0.03 \times 10$
1.63–1.90	1.69	$1.36 \pm 0.01 \pm 0.03 \times 10$	1.69	$1.16 \pm 0.01 \pm 0.03 \times 10$
1.90–2.20	1.96	$1.16 \pm 0.01 \pm 0.03 \times 10$	1.97	$9.79 \pm 0.07 \pm 0.22$
2.20–2.55	2.27	$9.84 \pm 0.06 \pm 0.21$	2.29	$8.13 \pm 0.06 \pm 0.17$
2.55–2.96	2.64	$8.09 \pm 0.05 \pm 0.16$	2.65	$6.64 \pm 0.05 \pm 0.13$
2.96–3.44	3.06	$6.57 \pm 0.04 \pm 0.13$	3.07	$5.36 \pm 0.04 \pm 0.11$
3.44–3.99	3.56	$5.21 \pm 0.04 \pm 0.10$	3.56	$4.21 \pm 0.03 \pm 0.08$
3.99–4.63	4.12	$4.14 \pm 0.03 \pm 0.08$	4.13	$3.24 \pm 0.03 \pm 0.06$
4.63–5.38	4.80	$3.14 \pm 0.02 \pm 0.06$	4.78	$2.53 \pm 0.02 \pm 0.05$
5.38–6.24	5.57	$2.42 \pm 0.02 \pm 0.04$	5.57	$1.87 \pm 0.02 \pm 0.03$
6.24–7.25	6.47	$1.78 \pm 0.02 \pm 0.03$	6.47	$1.39 \pm 0.01 \pm 0.02$
7.25–8.41	7.49	$1.30 \pm 0.01 \pm 0.02$	7.50	$1.01 \pm 0.01 \pm 0.02$
8.41–9.76	8.73	$9.48 \pm 0.10 \pm 0.16 \times 10^{-1}$	8.75	$7.16 \pm 0.09 \pm 0.12 \times 10^{-1}$
9.76–11.3	10.1	$6.83 \pm 0.08 \pm 0.19 \times 10^{-1}$	10.1	$5.31 \pm 0.07 \pm 0.15 \times 10^{-1}$
11.3–13.1	11.7	$4.81 \pm 0.06 \pm 0.13 \times 10^{-1}$	11.8	$3.60 \pm 0.05 \pm 0.10 \times 10^{-1}$
13.1–15.3	13.6	$3.29 \pm 0.05 \pm 0.09 \times 10^{-1}$	13.6	$2.55 \pm 0.04 \pm 0.07 \times 10^{-1}$
15.3–17.7	15.8	$2.31 \pm 0.04 \pm 0.06 \times 10^{-1}$	15.7	$1.83 \pm 0.03 \pm 0.05 \times 10^{-1}$
17.7–20.6	18.3	$1.55 \pm 0.03 \pm 0.04 \times 10^{-1}$	18.4	$1.22 \pm 0.02 \pm 0.03 \times 10^{-1}$
20.6–23.9	21.1	$1.07 \pm 0.02 \pm 0.03 \times 10^{-1}$	21.3	$8.25 \pm 0.19 \pm 0.23 \times 10^{-2}$
23.9–27.7	24.7	$7.21 \pm 0.16 \pm 0.20 \times 10^{-2}$	24.6	$5.79 \pm 0.15 \pm 0.16 \times 10^{-2}$
27.7–32.1	28.5	$4.81 \pm 0.12 \pm 0.13 \times 10^{-2}$	28.7	$3.63 \pm 0.11 \pm 0.10 \times 10^{-2}$
32.1–37.3	33.2	$3.18 \pm 0.09 \pm 0.09 \times 10^{-2}$	33.4	$2.46 \pm 0.08 \pm 0.07 \times 10^{-2}$
37.3–43.3	38.4	$2.10 \pm 0.07 \pm 0.06 \times 10^{-2}$	38.5	$1.69 \pm 0.06 \pm 0.05 \times 10^{-2}$
43.3–50.2	44.6	$1.45 \pm 0.05 \pm 0.04 \times 10^{-2}$	44.2	$1.12 \pm 0.05 \pm 0.03 \times 10^{-2}$
50.2–58.3	51.8	$9.85 \pm 0.41 \pm 0.28 \times 10^{-3}$	52.0	$7.03 \pm 0.35 \pm 0.20 \times 10^{-3}$
58.3–67.7	59.2	$5.85 \pm 0.29 \pm 0.17 \times 10^{-3}$	59.3	$4.83 \pm 0.27 \pm 0.14 \times 10^{-3}$
67.7–78.5	71.5	$3.77 \pm 0.22 \pm 0.11 \times 10^{-3}$	68.5	$2.90 \pm 0.19 \pm 0.08 \times 10^{-3}$
78.5–91.1	80.1	$2.29 \pm 0.16 \pm 0.07 \times 10^{-3}$	80.4	$2.03 \pm 0.15 \pm 0.06 \times 10^{-3}$
91.1–106.	91.7	$1.70 \pm 0.13 \pm 0.05 \times 10^{-3}$	92.8	$1.25 \pm 0.11 \pm 0.04 \times 10^{-3}$

5. Summary

We have measured absolute fluxes of atmospheric muons at the top of Mt. Norikura, Japan. It is located at an altitude of 2 770 m above sea level. The overall errors of our measurements are less than $\pm 10\%$. The absolute fluxes showed relatively good agreement with theoretical predictions calculated by using the DPMJET-III hadronic interaction model. The precise measurement of the atmospheric muons can modify the hadronic interaction model and improve accuracy of atmospheric neutrino calculations.

Acknowledgements

We would like to thank all staffs in the Norikura Observatory, ICRR, the University of Tokyo for their cooperation. We are indebted to M. Honda and K. Kasa-

hara for their Monte Carlo simulations and theoretical interpretations. This experiment was supported by Grants-in-Aid from the ministry of Education, Culture, Sport, Science and Technology, MEXT. We would like to thank ISAS and KEK for their continuous support and encouragement for the BESS experiment. The analysis was performed with the computing facilities at ICEPP, the University of Tokyo.

References

[1] T. Sanuki et al., Astrophys. J. 545 (2000) 1135.
[2] AMS Collaboration, J. Alcaraz et al., Phys. Lett. B 490 (2000) 27.
[3] AMS Collaboration, J. Alcaraz et al., Phys. Lett. B 494 (2000) 193.
[4] M. Motoki et al., astro-ph/0205344, submitted to Astropart. Phys.
[5] S. Orito, in: J. Nishimura, K. Nakamura, A. Yamamoto, Proc. ASTROMAG Workshop, KEK Report KEK87-19, KEK, Ibaraki, 1987, p. 111..
[6] A. Yamamoto et al., Adv. Space Res. 14 (1994) 75.
[7] Y. Asaoka et al., Nucl. Instrum. Methods A 416 (1998) 236.
[8] Y. Ajima et al., Nucl. Instrum. Methods A 443 (2000) 71.
[9] Y. Shikaze et al., Nucl. Instrum. Methods A 455 (2000) 596.
[10] M.A. Shea, D.F. Smart, in: Proc. 27th ICRC, Hamburg, 2001, p. 4063.
[11] K. Kasahara, in: Proc. 24th ICRC, Rome, 1995, p. 399, also, http://eweb.b6.kanagawa-u.ac.jp/~kasahara/ResearchHome/cosmosHome/index.html.
[12] H. Pi, Comput. Phys. Commun. 71 (1992) 173.
[13] S. Roesler, R. Engel, J. Ranft, SLAC-PUB-8740, hep-ph/0012252, unpublished.
[14] J.D. Sullivan, Nucl. Instrum. Methods 95 (1971) 5.
[15] R. Brun et al., GEANT—Detector Description and Simulation Tool, CERN program library, CERN, Geneva, 1994.
[16] M.P. De Pascal et al., J. Geophys. Res. 98 (1993) 3501.
[17] J. Kremer et al., Phys. Rev. Lett. 83 (1999) 4241.
[18] M. Honda et al., in: Proc. 27th ICRC, Hamburg, 2001, p. 1162.
[19] M. Honda et al., Phys. Rev. D 52 (1995) 4985.

Update

Physics Letters B

Volume 581, Issue 3–4, 19 February 2004, Page 272–273

DOI: https://doi.org/10.1016/j.physletb.2003.11.060

Available online at www.sciencedirect.com
SCIENCE DIRECT®
Physics Letters B 581 (2004) 272–273
PHYSICS LETTERS B
www.elsevier.com/locate/physletb

Erratum

Erratum to: "Measurements of atmospheric muon spectra at mountain altitude" [Phys. Lett. B 541 (2002) 234] ☆

T. Sanuki [a,*], M. Fujikawa [a], K. Abe [a], K. Anraku [a,1], Y. Asaoka [a,2], H. Fuke [a], S. Haino [a], M. Imori [a], K. Izumi [a], T. Maeno [b], Y. Makida [c], N. Matsui [a], H. Matsumoto [a], H. Matsunaga [a,3], M. Motoki [a,4], J. Nishimura [a], M. Nozaki [b], S. Orito [a,5], M. Sasaki [c,6], Y. Shikaze [b], T. Sonoda [a], J. Suzuki [c], K. Tanaka [c], Y. Toki [b], A. Yamamoto [c], Y. Yamamoto [a], K. Yamato [b], T. Yoshida [c], K. Yoshimura [c]

[a] *The University of Tokyo, Bunkyo, Tokyo 113-0033, Japan*
[b] *Kobe University, Kobe, Hyogo 657-8501, Japan*
[c] *High Energy Accelerator Research Organization (KEK), Tsukuba, Ibaraki 305-0801, Japan*

Received 28 November 2003

Due to a mistake in the tabulation, mean momentum ($\bar{P}$) in Table 1 should be corrected. This correction affects none of the figures given in the Letter.

Table 1
Absolute differential momentum spectra of atmospheric muons

Momentum range (GeV/c)	μ^+		μ^-	
	$\bar{P}$ (GeV/c)	Flux $\pm \Delta\text{Flux}_{\text{sta}} \pm \Delta\text{Flux}_{\text{sys}}$ $(\text{m}^2\,\text{sr}\,\text{s}\,\text{GeV}/c)^{-1}$	$\bar{P}$ (GeV/c)	Flux $\pm \Delta\text{Flux}_{\text{sta}} \pm \Delta\text{Flux}_{\text{sys}}$ $(\text{m}^2\,\text{sr}\,\text{s}\,\text{GeV}/c)^{-1}$
0.576–0.669	0.623	$2.39 \pm 0.02 \pm 0.09 \times 10$	0.623	$2.29 \pm 0.02 \pm 0.09 \times 10$
0.669–0.776	0.722	$2.29 \pm 0.02 \pm 0.08 \times 10$	0.723	$2.11 \pm 0.02 \pm 0.07 \times 10$

(*continued*)

☆ doi of original article: 10.1016/S0370-2693(02)02265-7.
* Corresponding author.
E-mail address: sanuki@phys.s.u-tokyo.ac.jp (T. Sanuki).
1 Present address: Kanagawa University, Yokohama, Kanagawa 221-8686, Japan.
2 Present address: ICRR, The University of Tokyo, Kashiwa, Chiba 227-8582, Japan.
3 Present address: University of Tsukuba, Tsukuba, Ibaraki 305-8571, Japan.
4 Present address: Tohoku University, Sendai, Miyagi 980-8578, Japan.
5 Deceased.
6 Present address: National Aeronautics and Space Administration, Goddard Space Flight Center, Greenbelt, MD 20771, USA.

doi:10.1016/j.physletb.2003.11.060

Table 1 (*continued*)

Momentum range (GeV/c)	μ^+		μ^-	
	$\bar{P}$ (GeV/c)	Flux $\pm$ ΔFlux$_{sta}$ $\pm$ ΔFlux$_{sys}$ (m^2 sr s GeV/c)$^{-1}$	$\bar{P}$ (GeV/c)	Flux $\pm$ ΔFlux$_{sta}$ $\pm$ ΔFlux$_{sys}$ (m^2 sr s GeV/c)$^{-1}$
0.776–0.901	0.839	$2.17 \pm 0.02 \pm 0.07 \times 10$	0.838	$1.99 \pm 0.02 \pm 0.06 \times 10$
0.901–1.05	0.972	$2.03 \pm 0.02 \pm 0.06 \times 10$	0.972	$1.83 \pm 0.01 \pm 0.05 \times 10$
1.05–1.21	1.13	$1.89 \pm 0.01 \pm 0.05 \times 10$	1.13	$1.70 \pm 0.01 \pm 0.05 \times 10$
1.21–1.41	1.31	$1.73 \pm 0.01 \pm 0.05 \times 10$	1.31	$1.53 \pm 0.01 \pm 0.04 \times 10$
1.41–1.63	1.52	$1.54 \pm 0.01 \pm 0.04 \times 10$	1.52	$1.33 \pm 0.01 \pm 0.03 \times 10$
1.63–1.90	1.76	$1.36 \pm 0.01 \pm 0.03 \times 10$	1.76	$1.16 \pm 0.01 \pm 0.03 \times 10$
1.90–2.20	2.05	$1.16 \pm 0.01 \pm 0.03 \times 10$	2.04	$9.79 \pm 0.07 \pm 0.22$
2.20–2.55	2.37	$9.84 \pm 0.06 \pm 0.21$	2.37	$8.13 \pm 0.06 \pm 0.17$
2.55–2.96	2.75	$8.09 \pm 0.05 \pm 0.16$	2.75	$6.64 \pm 0.05 \pm 0.13$
2.96–3.44	3.19	$6.57 \pm 0.04 \pm 0.13$	3.19	$5.36 \pm 0.04 \pm 0.11$
3.44–3.99	3.71	$5.21 \pm 0.04 \pm 0.10$	3.71	$4.21 \pm 0.03 \pm 0.08$
3.99–4.63	4.30	$4.14 \pm 0.03 \pm 0.08$	4.30	$3.24 \pm 0.03 \pm 0.06$
4.63–5.38	4.99	$3.14 \pm 0.02 \pm 0.06$	4.99	$2.53 \pm 0.02 \pm 0.05$
5.38–6.24	5.79	$2.42 \pm 0.02 \pm 0.04$	5.79	$1.87 \pm 0.02 \pm 0.03$
6.24–7.25	6.72	$1.78 \pm 0.02 \pm 0.03$	6.71	$1.39 \pm 0.01 \pm 0.02$
7.25–8.41	7.80	$1.30 \pm 0.01 \pm 0.02$	7.80	$1.01 \pm 0.01 \pm 0.02$
8.41–9.76	9.05	$9.48 \pm 0.10 \pm 0.16 \times 10^{-1}$	9.05	$7.16 \pm 0.09 \pm 0.12 \times 10^{-1}$
9.76–11.3	10.5	$6.83 \pm 0.08 \pm 0.19 \times 10^{-1}$	10.5	$5.31 \pm 0.07 \pm 0.15 \times 10^{-1}$
11.3–13.1	12.2	$4.81 \pm 0.06 \pm 0.13 \times 10^{-1}$	12.2	$3.60 \pm 0.05 \pm 0.10 \times 10^{-1}$
13.1–15.3	14.1	$3.29 \pm 0.05 \pm 0.09 \times 10^{-1}$	14.2	$2.55 \pm 0.04 \pm 0.07 \times 10^{-1}$
15.3–17.7	16.4	$2.31 \pm 0.04 \pm 0.06 \times 10^{-1}$	16.4	$1.83 \pm 0.03 \pm 0.05 \times 10^{-1}$
17.7–20.6	19.0	$1.55 \pm 0.03 \pm 0.04 \times 10^{-1}$	19.0	$1.22 \pm 0.02 \pm 0.03 \times 10^{-1}$
20.6–23.9	22.1	$1.07 \pm 0.02 \pm 0.03 \times 10^{-1}$	22.1	$8.25 \pm 0.19 \pm 0.23 \times 10^{-2}$
23.9–27.7	25.6	$7.21 \pm 0.16 \pm 0.20 \times 10^{-2}$	25.6	$5.79 \pm 0.15 \pm 0.16 \times 10^{-2}$
27.7–32.1	29.8	$4.81 \pm 0.12 \pm 0.13 \times 10^{-2}$	29.8	$3.63 \pm 0.11 \pm 0.10 \times 10^{-2}$
32.1–37.3	34.5	$3.18 \pm 0.09 \pm 0.09 \times 10^{-2}$	34.6	$2.46 \pm 0.08 \pm 0.07 \times 10^{-2}$
37.3–43.3	39.9	$2.10 \pm 0.07 \pm 0.06 \times 10^{-2}$	40.1	$1.69 \pm 0.06 \pm 0.05 \times 10^{-2}$
43.3–50.2	46.5	$1.45 \pm 0.05 \pm 0.04 \times 10^{-2}$	46.6	$1.12 \pm 0.05 \pm 0.03 \times 10^{-2}$
50.2–58.3	54.1	$9.85 \pm 0.41 \pm 0.28 \times 10^{-3}$	53.9	$7.03 \pm 0.35 \pm 0.20 \times 10^{-3}$
58.3–67.7	62.7	$5.85 \pm 0.29 \pm 0.17 \times 10^{-3}$	62.6	$4.83 \pm 0.27 \pm 0.14 \times 10^{-3}$
67.7–78.5	73.2	$3.77 \pm 0.22 \pm 0.11 \times 10^{-3}$	72.3	$2.90 \pm 0.19 \pm 0.08 \times 10^{-3}$
78.5–91.1	84.5	$2.29 \pm 0.16 \pm 0.07 \times 10^{-3}$	84.6	$2.03 \pm 0.15 \pm 0.06 \times 10^{-3}$
91.1–106.	97.4	$1.70 \pm 0.13 \pm 0.05 \times 10^{-3}$	97.3	$1.25 \pm 0.11 \pm 0.04 \times 10^{-3}$